Proceedings of PVP2006
2006 ASME Pressure Vessels and Piping Division Conference
July 23-27, 2006, Vancouver, British Columbia, Canada
PVP2006-ICPVT11-93730

ELECTROCHEMICAL TESTING OF GAS TUNGSTEN ARC WELDED AND REDUCED PRESSURE ELECTRON BEAM WELDED ALLOY 22

S. Daniel Day, Frank M. G. Wong, Steven R. Gordon, Lana L. Wong and Raul B. Rebak

Lawrence Livermore National Laboratory
7000 East Ave, L-631
Livermore, California, 94550 USA

ABSTRACT

Alloy 22 (N06022) is the material selected for the fabrication of the outer shell of the nuclear waste containers for the Yucca Mountain high-level nuclear waste repository site. A key technical issue in the waste package program has been the integrity of the container weld joints. The currently selected welding process for fabricating and sealing the containers is the traditional gas tungsten arc welding (GTAW) or TIG method. An appealing faster alternative technique is reduced pressure electron beam (RPEB) welding. It was of interest to compare the corrosion properties of specimens prepared using both types of welding techniques. Standard electrochemical tests were carried on GTAW and RPEB welds as well as on base metal (non-welded) to determine their relative corrosion behavior in simulated concentrated water (SCW) at 90°C (alkaline), 1 M HCl at 60°C (acidic) and 1 M NaCl at 90°C (neutral) solutions. Results show that for all practical purposes, the three tested materials had the same electrochemical behavior in the three tested electrolytes.

Keywords: N06022, Gas Tungsten Arc Welding, Reduced Pressure Electron Beam Welding, General Corrosion, Localized Corrosion

INTRODUCTION

Alloy 22 (N06022) is the material selected for the fabrication of the outer shell of the nuclear waste containers for the Yucca Mountain nuclear waste repository site [1]. The selection has been based on its overall resistance to corrosion in both oxidizing and reducing environments, and its successful use in extremely aggressive industrial applications. Alloy 22 has been shown to have a much greater resistance than conventional stainless steel grades to pitting corrosion and stress corrosion cracking in chloride-bearing environments [2-3]. Extensive welding will be used to fabricate the containers. The outer shell is expected to have three circumferential and one longitudinal weld seams. Roughly, each container will have more than 25 m of weld seam that would be exposed to the environment at the permanent emplacement site. In industrial applications it is generally regarded that weld seams are the most vulnerable section in a given equipment since welds can be sites of residual stress that could promote stress corrosion cracking and metallurgical heterogeneity that could promote localized corrosion under favorable electrochemical and environmental conditions. The current candidate welding process to fabricate the waste container is the classic gas tungsten arc welding (GTAW) or TIG technique. Another appealing procedure is the reduced pressure electron beam (RPEB) method developed in the United Kingdom. The RPEB welding method is particularly appealing for the welding of thick plates since it requires only one pass as compared to multiple passes for the GTAW. Other benefits are that RPEB does not require filler metal and does not require extensive plate machining prior to welding.

Figure 1 shows a macrograph of the cross section of a 1.5-inch thick Alloy 22 plate that was welded using the GTAW technique. This was a double V welding that consisted of at least nine passes on each side of the plate. Figure 1 shows that the width of the weld seam was up to 20 mm in the outside surface and approximately 10 mm wide in the middle section of each V (at one fourth of the plate thickness). Figure 2 shows a macrograph of the cross section of a 1.5-inch thick plate that was welded using the RPEB technique. This was a single pass autogenous weld, with a maximum width at the surface of 10 mm and a rather constant weld seam width through the

thickness of the plate of 3 mm. Comparing Figures 1 and 2, it is obvious that the RPEB plate contains less amount of weld material than the GTAW plate.

The current study was undertaken to examine the relative corrosion resistance of Alloy 22 in three conditions: (1) base metal, (2) GTAW and (3) RPEB. The general and localized corrosion studies of the three types of material were carried out in three different electrolyte solutions. These were Simulated Concentrated Water (SCW), One Molar Hydrochloric Acid (1 M HCl) and One Molar Sodium Chloride (1 M NaCl) solutions. SCW was used as a representative concentrated ground water since SCW is approximately 1000 times more concentrated than the J-13 well water from near Yucca Mountain. SCW is slightly alkaline (pH between 8 and 10). The 1 M HCl at 60°C environment was used since it can etch welds under positive polarization. The pH of 1 M HCl is zero (highly acidic). The saline solution 1 M NaCl at 90°C was used since it can promote crevice corrosion in Alloy 22 under anodic applied potentials. The pH of 1 M NaCl is near neutral.

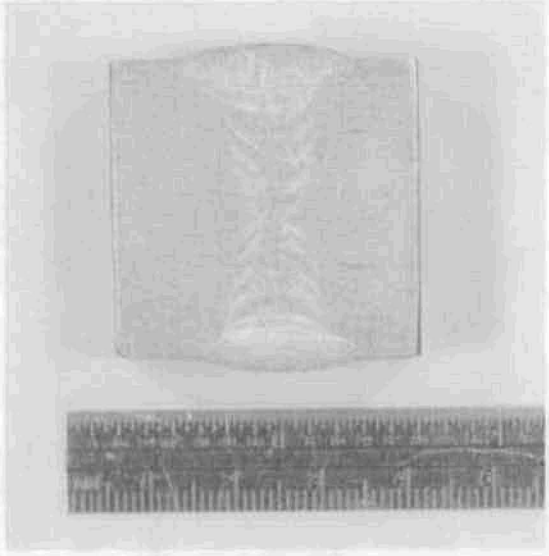

Figure 1. Macrograph of a GTAW welded Alloy 22 plate

EXPERIMENTAL

The test specimens were water jet-cut from a 1.25-inch thick Alloy 22 plate containing GTAW and RPEB weld seams. Framatome (USA) performed the GTAW welding and the TWI (UK) carried out the RPEB welding. The heat of the base metal was 059902LL1 and the heat of the weld wire used for the GTAW was XX1753BG. The compositions of these heats are given in Table 1 (See also ASTM B 575) [4]. The different specimens were manufactured by CTC-United Defense (now BAE Systems) in Santa Clara, CA and surface finished at Lawrence Livermore National Laboratory (LLNL). There were two type of specimens, discs (per ASTM G 5) [5] and standard MCA (multiple crevice assembly) specimens. The discs were prepared from five cores taken through the weld plate from the beam or arc side to the opposite surface. Four discs were sliced from each core, one from the top surface (A) and one from the bottom surface (D), and two from locations one-third (B) and two-thirds (C) the distance from the top surface A. The specimens used in this study were from the top surface (A) and the one-third depth level (B) beneath it. The GTAW weld specimen series was designated GXXX and the RPEM weld series 15XXX. Separate Alloy 22 base metal disks in the mill-annealed (MA) condition that were not taken from this welded plates were labeled DEAXXXX. The MCA specimens lie in the plate plane with the weld seams cutting across the loop end, perpendicular to the stem direction (Figure 3). The MCA specimens were taken from the same sampling levels (A through D) as the disks.

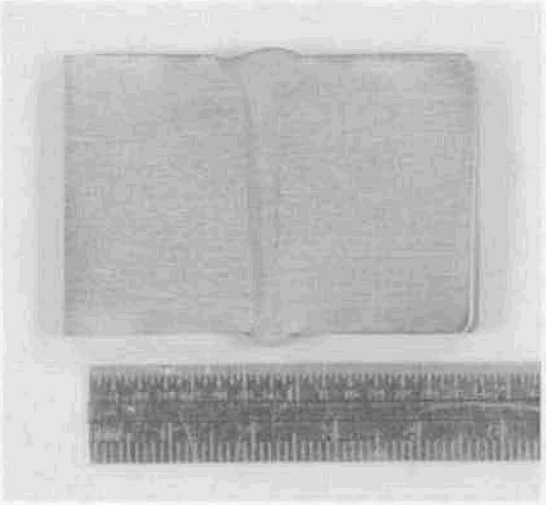

Figure 2. Macrograph of a RPEB welded Alloy 22 plate

Most of the test specimens were discs designed to test for general corrosion and passivity according to ASTM G 61 guidelines. The discs were 0.625-inch diameter. In the case of GTAW, most of the disc was weld metal. In the case of RPRB only about one third of the exposed surface was weld metal. The MCA specimens were assembled using a Teflon-coated ceramic washer for crevice forming as described in ASTM G 48 [5] (Figure 3). The tested surface area of the disc specimens was approximately 0.7 cm^2 and the exposed MCA specimen area was about 5.6 cm^2. The test specimens were given a 600 grit silicon carbide abrasive paper finish approximately one hour prior to testing. They were then ultrasonicated in distilled

water for 5 minutes and then degreased with acetone, isopropyl alcohol, and distilled water.

Table 1.
Chemical Composition of the Studied Materials

Element	Base Metal 1.25-inch thick Plate (Heat 059902LL1 by Allegheny Ludlum)	Filler Metal 0.045-inch dia. Wire for GTAW (Heat XX1753BG by Inco Alloys International)
C	0.005	0.004
Co	0.01	0.03
Cr	20.38	20.54
Cu	0.01	0.04
Fe	2.85	2.08
Mn	0.16	0.2
Mo	13.82	14.00
Ni	59.56	59.70
P	0.008	0.004
S	0.0002	0.001
Si	0.05	0.06
V	0.17	0.03
W	2.64	3.10

Electrochemical tests were carried out in deaerated solutions of SCW (Table 2), 1 M HCl, and 1 M NaCl. The SCW has a pH of about 9-10. The pH of the NaCl solution was approximately 7 and the hydrochloric acid solution had a pH of 0. The SCW and 1 M NaCl test temperature was 90°C and the 1 M HCl tests were carried out at 60°C. Nitrogen (N_2) was bubbled through the solution at a flow rate of 100 cc/min for the duration of the electrochemical tests. The corrosion potential (E_{corr}) was monitored for 1 hour, and was immediately followed by three consecutive polarization resistance (PR) tests (ASTM G 59) [5] and one cyclic potentiodynamic polarization (CPP) test (ASTM G 61) [5].

Table 2.
Chemical Comp. of the SCW Solution (mg/L)

K^+	Na^+	Mg^{2+}	Ca^{2+}	F^-
3400	40,900	<1	<1	1400

Cl^-	NO_3^-	SO_4^{2-}	HCO_3^-	$SiO_{2\,(aq)}$
6700	6400	16,700	70,000	~40

The electrochemical tests were carried out in a one-liter, three-electrode, borosilicate glass flask (ASTM G 5). A water-cooled condenser combined with a water trap was used to avoid evaporation of the solution and the ingress of air. Solution temperatures were maintained by partially immersing the cell in a thermostat-controlled silicone oil bath. All the tests were conducted at ambient pressure. The reference electrode was a saturated silver chloride (SSC) electrode, which has a potential 199 mV more positive than the standard hydrogen electrode (SHE). The reference electrode was connected to the solution through a water-cooled Luggin probe to keep it near ambient temperature. The counter electrode was a flag (36 cm^2) of platinum foil spot-welded to a platinum wire. All the potentials in this paper are reported in the SSC scale.

The corrosion rates (CR) were obtained using the polarization resistance method (ASTM G 59) [5]. An initial applied voltage 20 mV below the corrosion potential (E_{corr}) was ramped up to a final potential of 20 mV above E_{corr} at a rate of 0.167 mV/s. Linear fits were constrained to a potential range of 10 mV below E_{corr} to 10 mV above E_{corr}. The fitting of the potential vs. current curves allows the calculation of the polarization resistance (Rp). The Tafel constants, ba and bc, were assumed to be ± 0.12 V/decade. Corrosion rates were calculated using the following equations

$$i_{corr} = \frac{1}{R_p} \times \frac{b_a \cdot b_c}{2.303(b_a + b_c)} = \frac{B}{R_p} = \frac{0.026}{R_p}$$

$$CR(\mu m / yr) = k \frac{i_{corr}}{\rho} EW$$

where k is a conversion factor (3.27 x 10^6 µm·g·/A·cm·yr), i_{corr} is the measured corrosion current density in A/cm^2, EW is the equivalent weight (23.28 g/mol), and ρ is the density of Alloy 22 (8.69 g/cm^3).

Tests to assess the susceptibility of the Alloy 22 welds to localized corrosion and passive stability were conducted using the cyclic potentiodynamic polarization (CPP) technique (ASTM G 61) [5]. The potential scans began 50 mV below E_{corr} using a set scan rate of 0.167 mV/s. The scan direction was usually reversed when the current density reached 5 mA/cm^2 in the forward scan. After the cyclic polarization tests the specimens were examined in an optical stereomicroscope at a 40X magnification to establish the mode of attack. Selected specimens were also imaged using a scanning electron microscope (SEM).

One specimen of each weld type (GTAW and RPEB) was subjected to galvanostatic (constant current density) testing in the HCl solution to reveal weld areas that were more susceptible to corrosion. The galvanostatic tests were preceded by a 1-hour open circuit potential run and three linear polarizations scans to measure corrosion rates. The galvanostatic procedure passes current through the specimen to maintain a fixed current density for a given length of time. The initial test pair (G04A and 1504A) was exposed to a current density of 0.1 mA/cm^2 for 3 hours. The resulting corrosion features were mild enough to require a second test at a higher current density of 1 mA/cm^2 using specimens G03A and

1503A. The latter specimens showed significant corrosion features to merit SEM imaging and EDS analysis. The images and major element compositional data will be used to document the susceptibility of different regions or phase domains in the welds to generalized corrosion.

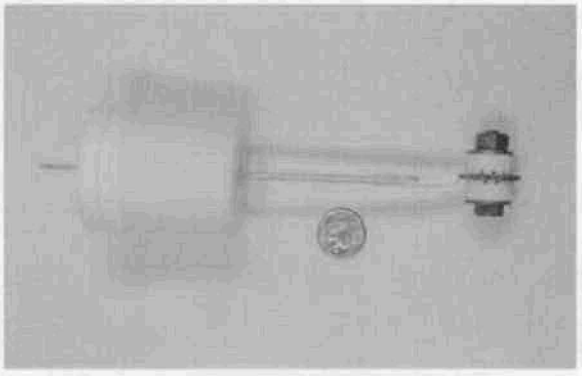

Figure 3. MCA Specimen for Crevice Corrosion Testing

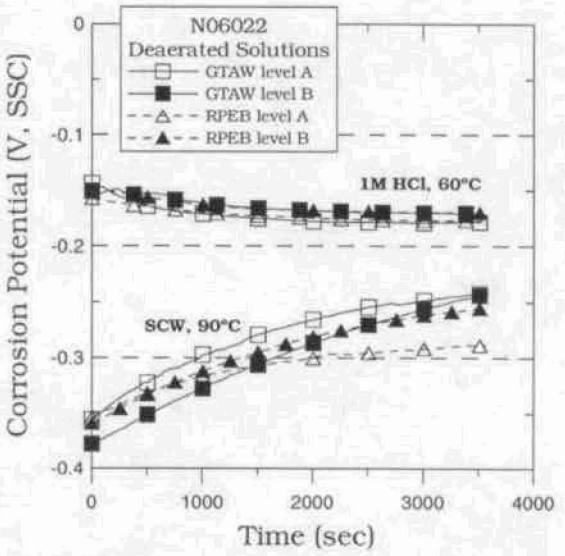

Figure 4. Short-term evolution of E_{corr} in time

RESULTS AND DISCUSSION

Corrosion Potential

Figure 4 shows the evolution of E_{corr} for GTAW and RPEB welded material discs in SCW and 1 M HCl solution. A one-hour interval may not be sufficient for the corrosion potential to reach a steady state value. A full comparison of the E_{corr} evolution between solution and solution is not possible since 1 M HCl was at 60°C and the other two (NaCl and SCW) were at 90°C. In general, E_{corr} initially increased in the SCW and 1 M NaCl solution (not shown), and decreased in the 1 M HCl solution. The amount of change was more pronounced in the SCW and 1 M NaCl solution. These two latter solutions are not as corrosive as the 1 M HCl solution and therefore, E_{corr} increased as a protective oxide film was forming on the surface of the specimens. Figure 4 shows that the E_{corr} values are highly reproducible between run and run, especially for the 1 M HCl solution.

Figure 4 also shows the E_{corr} for each type of weld at the two different levels tested. Level A corresponded to the outermost layer of the plate and level B was the following level. Since the SCW solution is not as corrosive, there was not a clear trend on the values of E_{corr} based on the type of weld. Similarly, there was not a specific trend on the E_{corr} based on the level (A or B) the specimen was removed from in each weld condition (GTAW and RPEB). Figure 4 also shows that in the HCl solution, it appears that the level A specimens (both for GTAW and RPEB) were slightly more active than the level B specimens. However, there is not a clear trend between the two types of weld.

Table 3 and Figure 5 show the E_{corr} values after a 1 h immersion for discs (in HCl and SCW) and MCA specimens (in NaCl). The E_{corr} for the base MCA are for 24 h immersion. The E_{corr} for Alloy 22 in HCl solution are highly reproducible and non-dependent on the type of material (GTAW, RPEB or Base). For the SCW and NaCl solutions, the values of E_{corr} were less reproducible (because the solutions are less aggressive); however, it appears that the welds were more noble (higher E_{corr}) than the base material. The corrosion potentials given in Figure 5 and Table 3 are short-term and in deaerated solutions. They are not meant to represent the long-term corrosion potential of Alloy 22 in aerated environments.

Corrosion Rates

Table 3 shows corrosion rates as a function of the type of material in SCW at 90°C, 1 M HCl at 60°C and 1 M NaCl at 90°C solutions. These are short term corrosion rates for comparative purposes between material and material. The corrosion rates do not represent the long-term behavior of Alloy 22 in the given solutions. Figure 6 shows the corrosion rates for the three types of material (GTAW, RPEB and Base discs) in SCW at 90°C (Table 3). Figure 6 shows that the lowest corrosion rate corresponded to the base metal with an average value of 0.8 µm/year. The second lowest corrosion rate corresponded to the GTAW material with an average value of 1.3 µm/year and the highest corrosion rate corresponded to the RPEB material with an average corrosion rate of 2 µm/year.

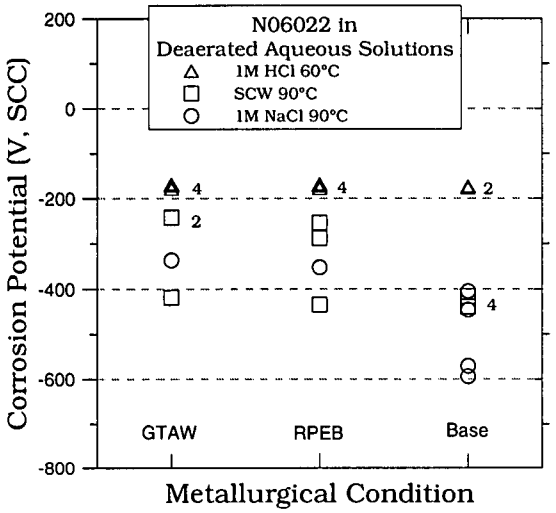

Figure 5. E_{corr} after 1 h (SCW and HCl) and 24-h (NaCl) immersion for all the studied materials (numbers indicate data points)

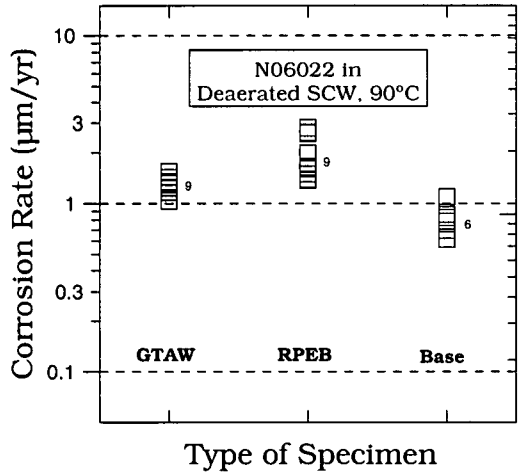

Figure 6. Corrosion rate for the three type of specimens in 90ºC SCW. Numbers indicate data points in each cluster. Data from Table 3

Figure 7 shows the corrosion rates for the three types of material (GTAW, RPEB and Base discs) in 1 M HCl at 60°C (Table 3). In this aggressive environment, the lowest corrosion rate corresponded to GTAW with an average value of 280 µm/year. The second lowest corrosion rate corresponded to the RPEB material with an average value of 335 µm/year and the highest corrosion rate corresponded to the base metal with and average value of 380 µm/year. This behavior was totally unpredictable since it was initially assumed that the welds would corrode faster in this acidic solution.

Figure 8 shows the corrosion rates for the three types of material (GTAW, RPEB and Base MCA specimens) in 1 M NaCl at 90°C (Table 3). In this saline solution the lowest corrosion rate also corresponded to the GTAW material with an average value of 0.6 µm/year. The second lowest corrosion rate was for the RPEB material with an average value of 0.8 µm/year and the highest corrosion rate was for the base material with an average value of 1.9 µm/year.

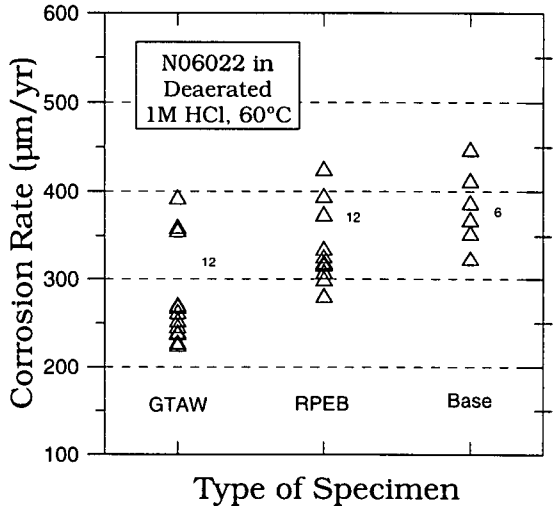

Figure 7. Corrosion rate for the three type of specimens in 1 M HCl at 60°C. Numbers indicate data points in each cluster. Data from Table 3

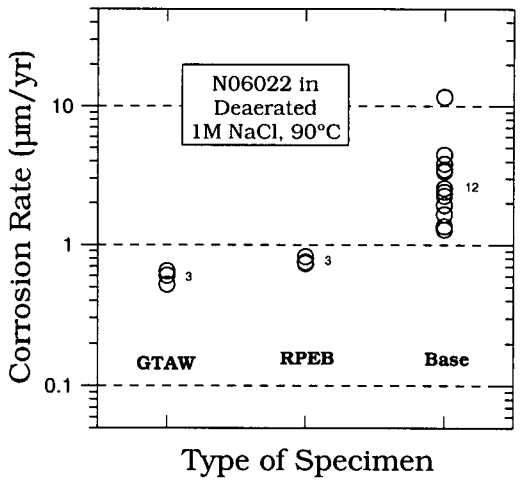

Figure 8. Corrosion rate for the three type of specimens in 1 M NaCl at 90ºC. Numbers indicate data points in each cluster. Data from Table 3

Figures 6-8 show that the corrosion rate in the 1 M HCl solution was approximately two orders of magnitude higher than in the other two less aggressive solutions. The overall

lowest corrosion rates were for the 1 M NaCl solution on MCA (creviced) specimens.

Cyclic Potentiodynamic Polarization (CPP)

Figures 9-11 show the cyclic polarization behavior of Alloy 22 GTAW, RPEB, and base metal specimens in deaerated SCW at 90°C, 1 M HCl at 60°C, and 1 M NaCl at 90°C solutions, respectively. For each solution, the cyclic polarization curves appear almost undistinguishable from each other for the three types of material (GTAW, RPEB and base). Figure 9 shows that for the SCW at 90°C solution, the cyclic polarization curves for all the materials show an anodic peak on the forward sweep at a potential of approximately 250 mV (SSC) with a current density between 350 to 550 μA/cm2. The highest current density was for the base material and the lowest for the GTAW specimen. The origin of these peaks is still unknown. There is also some noise in the final portion of the reverse scan where it crosses the forward passive region. The origin of this noise is also not known. Even though Figure 9 shows a small hysteresis in the reverse potential scanning, none of the materials tested in SCW at 90°C showed localized corrosion.

Characterization studies in the SEM after the cyclic polarization experiments in SCW at 90°C showed that the GTAW specimen had fewer amount of cavities on the surface than the RPEB specimen. Moreover, the cavities in the GTAW specimen seemed random while the cavities in the RPEB specimen seemed aligned, probably following freezing patterns in the weld pool.

Figure 10 shows that the cyclic polarization curves for the three materials in 1 M HCl at 60°C almost completely overlap. The largest current density for the anodic peak above the corrosion potential corresponded to the RPEB material (Figure 10). The breakdown potentials (E20 and E200 in Table 3) in 1 M HCl were almost identical for all three materials and well above +0.9 V SSC. None of the materials showed localized corrosion (pitting corrosion) after the potentiodynamic tests despite they were polarized to high anodic potentials in a 1 M chloride solution of pH = 0.

Figure 11 shows the cyclic polarization curves for GTAW and RPEB materials in 1 M NaCl at 90°C. Both curves were similar to each other and exhibited a reverse scan hysteresis loop that intersected the passive current line at –50 to –75 mV SSC. Microscopy of the specimens after the tests showed that both types of welded materials suffered crevice corrosion under the crevice formers. There was only one test for each welding condition so it is difficult to rank these two materials regarding their relative resistance to localized corrosion. In both types of materials the crevice corrosion nucleated and developed both in the welded part of the specimen and also in the base metal. This was easier to observe in the RPEB material since the weld seam was narrower.

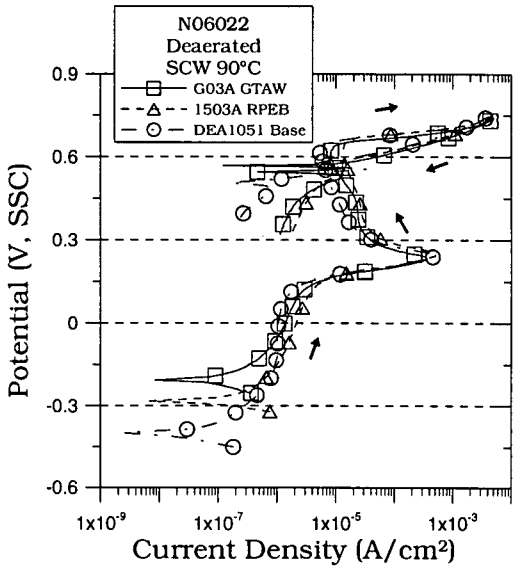

Figure 9. CPP for Three Different Alloy 22 Specimens in SCW solution at 90°C

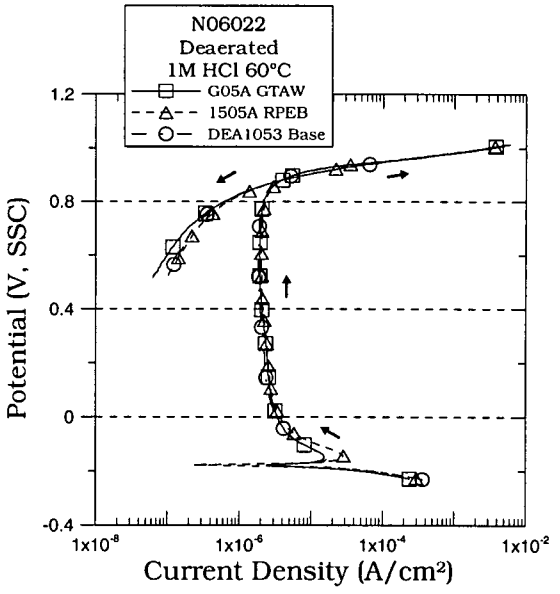

Figure 10. CPP for Three Different Alloy 22 Specimens in 1 M HCl solution at 60°C

Figure 12 show a SEM image of the localized corrosion in the GTAW specimen and Figures 13 and 14 show SEM images of the localized corrosion in the RPEB specimen. Figure 13 shows the band of the weld seam and the outline of one of the crevice formers. It is apparent that crevice corrosion nucleated not only at the boundary between the base metal and the weld seam but also in the base metal away from the weld seam. That is, there was not preferential attack by crevice corrosion in the weld seam.

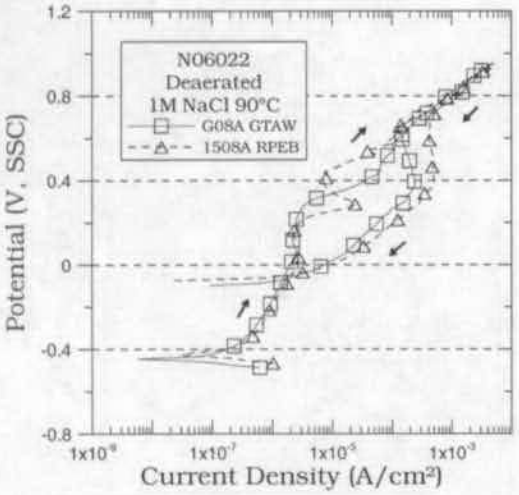

Figure 11. CPP for Two Welded and Creviced Alloy 22 Specimens in 1 M NaCl solution at 90°C

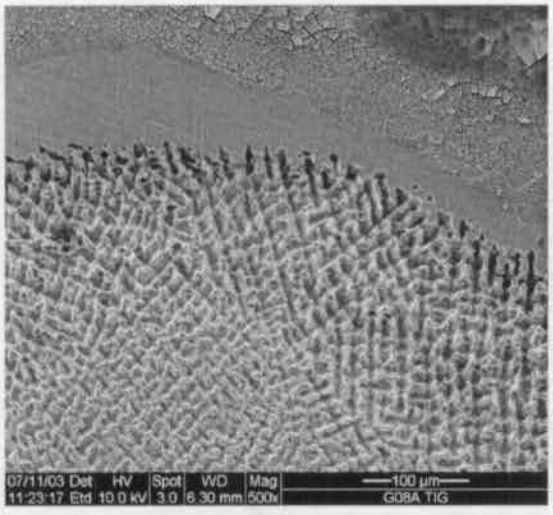

Figure 12. Localized corrosion in GTAW specimen G08A in 1 M NaCl at 90°C, 500 X Magnification

Characteristic Potentials from the CPP

In polarization curves (e.g. Figure 11) several specific potential values can be measured. These characteristic potentials are listed in Table 3. They can be divided between breakdown potentials (E20 and E200) and repassivation potentials (ER10 and ER1) (see Table 3 for description).

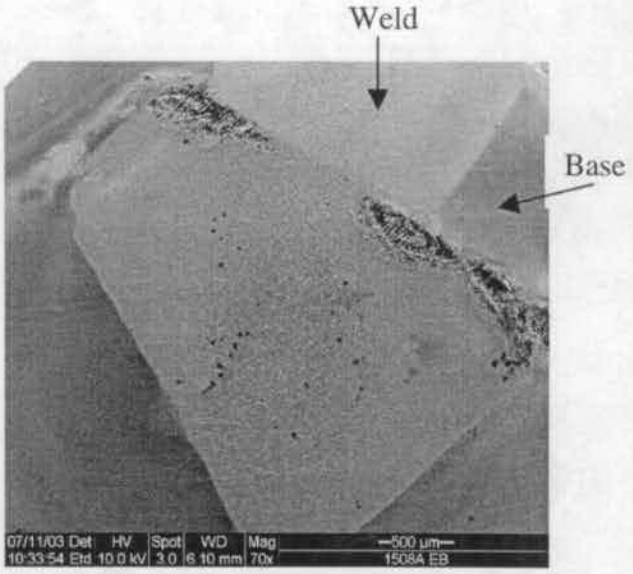

Figure 13. Localized corrosion in RPEB specimen 1508A in 1 M NaCl at 90°C, 70 X Magnification

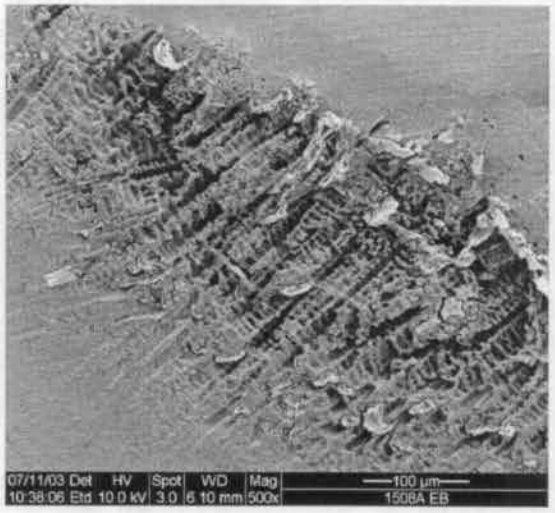

Figure 14. Localized corrosion in RPEB specimen 1508A in 1 M NaCl at 90°C, 500 X Magnification

The analysis of the parameters from the polarization curves will be done just for the 1 M NaCl solution since this was the only solution that promoted localized corrosion. Figure 15 shows the E_{corr} and ER10 (Table 3) in 1 M NaCl at 90°C. Figure 15 shows that the margin between E_{corr} and the repassivation potential is large for all three materials. The larger this difference the less prone the material will be to localized corrosion in the environment of testing. Both welded materials (GTAW and RPEB) had similar values of ΔE; however, these values correspond to only one tested specimen of each welded material. These preliminary results indicate that crevice corrosion would not occur in Alloy 22 base and welded at the corrosion potential under the tested conditions. A polarization

of several hundred mV (Figures 11 and 15) would be needed for localized corrosion to nucleate and propagate.

Galvanostatic Studies

Galvanostatic studies were carried to etch the weld seam in GTAW and RPEB specimens. Two sets of experiments were carried out in 1 M HCl solution at 60°C. In the first set, a current density of 0.1 mA/cm² was applied to the specimens for 3 h. In the second set, a ten times higher current density of 1 mA/cm² was applied for the same period. Figure 16 shows the potential output plots for the two applied constant current density tests. Both types of weld show the same applied potential for each applied current density. At the higher applied current density, the output potential was slightly higher (~ 30 mV) for both types of welds (Figure 25). The values of output potential are the same as in the polarization curve (Figure 15).

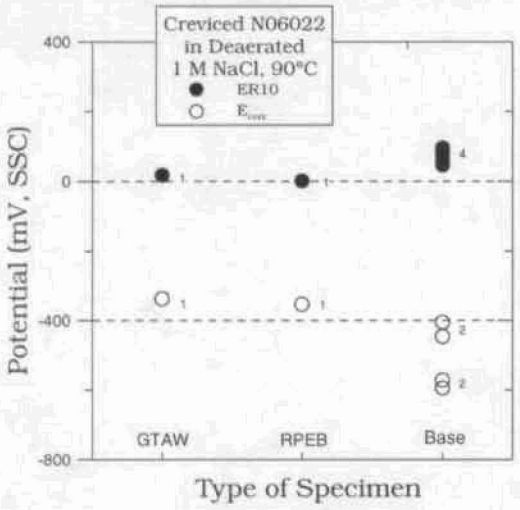

Figure 15. E_{corr} and ER10 for Alloy 22 in 1 M NaCl at 90°C

Figures 17 and 18 show the macro appearance of the corroded RPEB and GTAW specimens after the galvanostatic tests for the 1 mA/cm² applied current density. Figures 17 and 18 show that both weld seams were preferentially etched. Figure 17 shows that the weld seam in the RPEB welded specimen was much narrower than the weld seam in the GTAW specimen (Figure 18). This agrees with the macro-etch appearances of the cross section of the weld (Figures 1 and 2).

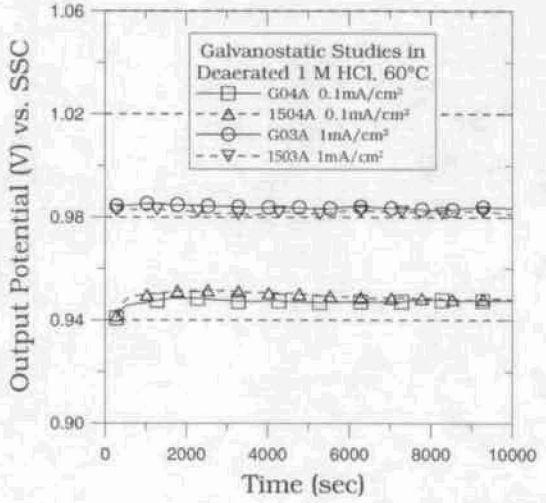

Figure 16. Galvanostatic Treatment under two applied currents for welded specimens in 1 M HCl at 60°C

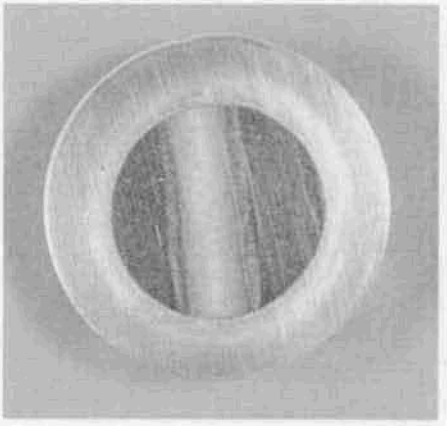

Figure 17. Specimen 1503A (RPEB) after galvanostatic treatment of 1 mA/cm² for 3 h in 1 M HCl at 60°C

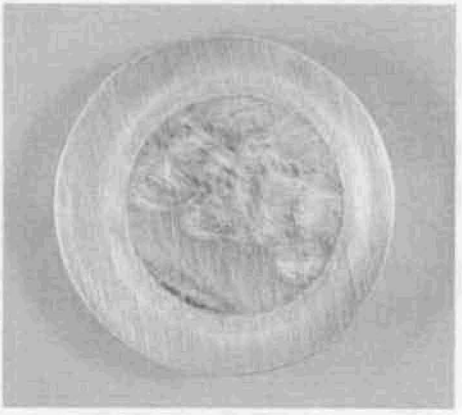

Figure 18. Specimen G03A (GTAW) after galvanostatic treatment of 1 mA/cm² for 3 h in 1 M HCl at 60°C

Figure 19 show a SEM image of the corroded RPEB welded specimen after the galvanostatic treatment. The corrosion pattern of the weld seam seems to follow specific directions, probably similar to those observed after the cyclic polarization in SCW solution. That is, by forcing the alloy to corrode at a constant current density, some areas of the weld seam appear to corrode preferentially to other areas (Figure 19). Figure 20 shows a SEM image of the corroded GTAW welded specimen after the galvanostatic treatment. Figure 20 shows a characteristic pattern of corrosion in the GTAW weld seam after the galvanostatic treatment. This was probably produced by the orientation of the cast structure of the weld.

Concluding Remarks

Preliminary work to evaluate the anodic behavior of Alloy 22 gas tungsten arc welds and reduced pressure electron beam welds in three test solutions has been completed. The test solutions were chosen to study the weld susceptibility to generalized corrosion, to localized/crevice corrosion, and to compare weld behavior in concentrated ground water solutions. No visible evidence of localized corrosion was seen in specimens from the SCW at 90°C and 1 M HCl at 60°C solutions, although passive film breakdown and repassivation were observed in the cyclic polarization scans. The 1 M NaCl at 90°C MCA tests showed crevice corrosion in both the weld zone and the base metal for each weld type. The GTAW specimens had slightly lower corrosion rates in the test solutions than the RPEB specimens. The GTAW specimens also had slightly more positive breakdown potential ranges above E_{corr} and larger critical potential gaps (ER10 potential minus E_{corr}) than the RPEB specimens. Although these imply superior stability under anodic conditions, the actual values for both welds were quite close in all the three solutions. A factor neglected in this testing was the effect of exposed weld area on specimen electrochemical behavior. This could be significant, since the tungsten arc welds were approximately twice the width of the electron beam welds. Additional work to characterize weld corrosion behavior using SEM-EDS microanalytical techniques could be used to improve the Alloy 22 electron beam welding process and capitalize on its desirable features for cost-effective waste container fabrication.

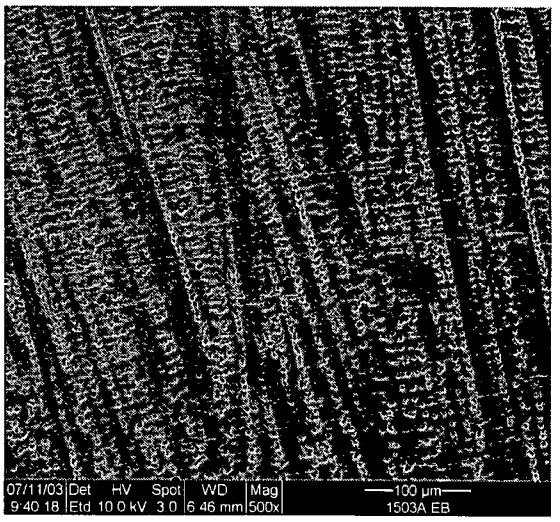

Figure 19. Corroded surface of RPEB specimen (1503A) after 1 mA/cm² galvanostatic testing in 1 M HCl at 60°C for 3 h, 500 X Magnification

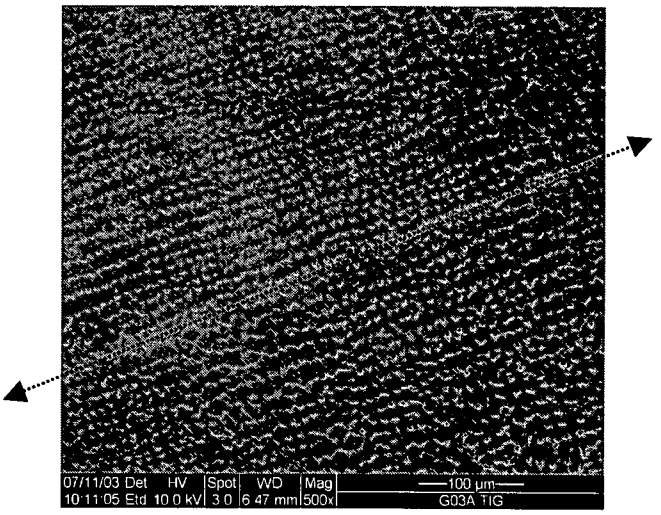

Figure 20. Corroded surface of GTAW specimen (G03A) after 1 mA/cm² galvanostatic testing in 1 M HCl at 60°C for 3 h, 500 X Magnification

CONCLUSIONS

- The Gas Tungsten Arc Welded (GTAW) weld seam was wider than the Reduced Pressure Electron Beam (RPEB) weld seam
- The short-term -Corrosion Potential (E_{corr}) in SCW and in 1 M NaCl solutions of the GTAW material was slightly more noble than for the RPEB and base materials. In the 1 M HCl solution, the short-term E_{corr} of all three materials was undistinguishable from each other.
- The corrosion rate of the RPEB welded specimens was of the same order of magnitude as the GTAW and the base materials.
- All three materials (GTAW, RPEB and Base) showed identical anodic behavior through cyclic polarization in acidic (HCl), neutral (NaCl) and alkaline (SCW) solutions.
- Both GTAW and RPEB welded material showed the same susceptibility to localized (crevice) corrosion in 1 M NaCl solutions. Moreover, in each material, the weld seam was not more susceptible to localized corrosion than the adjacent base metal.
- The corrosion pattern after the galvanostatic tests were oriented, typical of a cast structure of the weld seam.
- Overall, the electrochemical properties of the GTAW specimens were comparable to those of the RPEB weld specimens regarding passive film breakdown, film repassivation behavior, and corrosion rates. These observations are the result of laboratory testing only and may not represent any advantage from an industrial application point of view.

ACKNOWLEDGMENTS

This work was partially performed under the auspices of the U. S. Department of Energy by the University of California Lawrence Livermore National Laboratory under contract W-7405-Eng-48. The work was supported by the Yucca Mountain Project, which is part of the DOE Office of Civilian Radioactive Waste Management (OCRWM).

DISCLAIMER

REFERENCES

1. G. M. Gordon, Corrosion, 58, 811 (2002).
2. P. E. Manning, J. D. Schöbel, Werkstoffe und Korrosion, 37, 137-145 (1986).
3. R. B. Rebak in Corrosion and Environmental Degradation, Volume II, pp. 69-111 (Weinheim, Germany: Wiley-VCH 2000).
4. ASTM International, Annual Book of ASTM Standards, Volume 02.04 "Non-Ferrous Metals" Standard B-575 (West Conshohocken, PA: ASTM International, 2004).
5. ASTM International, Annual Book of ASTM Standards, Volume 03.02 "Wear and Erosion; Metal Corrosion" p. 91 (West Conshohocken, PA: ASTM International, 2004).

Table 3. Tested Conditions and Representative Potentials from CPP

Specimen ID (1)	Type of Material	Electrolyte, Temperature (°C)	1-h E_{corr} (mV, SSC)	Corrosion Rates (μm/year)	E20 (mV, SSC)	E200 (mV, SSC)	ER10 (mV, SSC)	ER1 (mV, SSC)
G01B	GTAW	SCW, 90°C	-418.6	1.232, 1.164, 1.034	170.4(AP), 648.2	668.1	571.9	568.6
G03A	GTAW	SCW, 90°C	-241.6	1.549, 1.351, 1.243	177.0(AP), 654.9	674.8	575.2	568.6
G03A (V)	GTAW	1M HCl, 60°C	-167.4	246.9, 238.8, 269.5	N/A	N/A	N/A	N/A
G03B	GTAW	SCW, 90°C	-242.5	1.431, 1.340, 1.315	180.3(AP), 651.5	674.8	575.2	558.6
G04A (V)	GTAW	1M HCl, 60°C	-171.5	357.1, 360.8, 393.8	N/A	N/A	N/A	N/A
G05A	GTAW	1M HCl, 60°C	-177.7	225.8, 253.7, 271.2	929.2	960.2	902.7	823.0
G05B	GTAW	1M HCl, 60°C	-170.4	228.4, 240.0, 263.2	929.2	955.8	902.7	823.0
G08A	GTAW	1M NaCl, 90°C	-337.2	0.649, 0.605, 0.522	362.8	678.1	17.7	-78.5
1501B	RPEB	SCW, 90°C	-434.8	1.999, 1.614, 1.652	N/A	N/A	N/A	N/A
1503A	RPEB	SCW, 90°C	-288.0	2.609, 2.645, 2.809	183.6(AP), 664.8	688.1	581.9	575.2
1503A (V)	RPEB	1M HCl, 60°C	-172.1	300.7, 308.5, 326.5	N/A	N/A	N/A	N/A
1503B	RPEB	SCW, 90°C	-254.3	1.499, 1.393, 1.373	183.6(AP), 671.5	691.4	588.5	581.9
1504A (V)	RPEB	1M HCl, 60°C	-167.6	316.7, 319.5, 336.0	N/A	N/A	N/A	N/A
1505A	RPEB	1M HCl, 60°C	-177.2	375.1, 395.8, 426.3	933.6	960.2	907.1	823.0
1505B	RPEB	1M HCl, 60°C	-170.0	281.6, 308.6, 318.3	924.8	955.8	902.7	823.0
1508A	RPEB	1M NaCl, 90°C	-353.1	0.754, 0.823, 0.737	269.9(AP), 488.9	691.4	1.1	-58.6
DEA1051	Base	SCW, 90°C	-439.3	0.786, 0.693, 0.611	183.6(AP), 664.8	688.1	588.5	568.6
DEA1052	Base	SCW, 90°C	-415.8	1.096, 0.859, 0.827	183.6(AP), 648.2	664.8	578.5	555.3
DEA1053	Base	1M HCl, 60°C	-176.1	369.2, 413.3, 448.1	924.8	955.8	902.7	827.4
DEA1054	Base	1M HCl, 60°C	-172.5	324.1, 353.8, 388.0	933.6	960.2	907.1	831.9
DEA3143	Base	1M NaCl, 90°C	-405	3.48, 4.45, 2.25	-251(AP), 510	740	64	-70
DEA3144	Base	1M NaCl, 90°C	-446	3.38, 3.84, 11.63	-277(AP), 503	722	46	-92
DEA3262	Base	1M NaCl, 90°C	-571	2.28, 1.59, 1.32	422	709	96	-72
DEA3263	Base	1M NaCl, 90°C	-594	2.77, 2.43, 1.28	386	703	81	-77

(1) For SCW and HCl solutions the specimens were discs and for the NaCl solution they were multiple crevice assemblies (MCA). (V) The specimen was used for galvanostatic test (Figure 16). All Specimens finished with 600-grit paper before testing. NA = Not Available or Not Applicable. Ecorr is the corrosion potential before starting the polarization tests, the Corrosion rate was obtained using the polarization resistance method and fitting the curves between ±10 mV around the corrosion potential. These corrosion rates are for comparative purposes only and they are not meant to represent the long term corrosion rate of Alloy 22 in the same electrolyte solutions. AP means anodic peak. E20 and E200 are the potentials in the forward scan for which the current density reaches 20 and 200 μA/cm² respectively. They represent values of breakdown potential. ER10 and ER1 are the potentials in the reverse scan for which the current density reaches 10 and 1 μA/cm². ER10 and ER1 represent values of repassivation potential.